GENERATION OF IRREGULAR COMPOSITE MICROSTRUCTURES THROUGH OPTIMIZATION

Matheus Urzedo Quirino[a], Volnei Tita[a], Marcelo Leite Ribeiro[a]

[a]São Carlos School of Engineering, University of São Paulo
Av. João Dagnone, 1100 – Jardim Santa Angelina, São Carlos, SP, Brazil – 13563-120
matheus.quirino@usp.br, voltita@sc.usp.br, malribei@usp.br

Keywords: composites materials, random microstructures, point process statistics, optimization.

1. INTRODUCTION

Composite materials are of general use nowadays, which may be justified by their resistances to corrosion and fatigue, as well as their specific stiffness and strength [1]. However, their structural integrity depends on failure mechanisms initiating at the material microstructure, which, in turn, lead to macrostructural effects [2], that is, effects at the coupon or component levels [3], therefore supporting the use of multiscale simulations.

These simulations require a microstructural model, regarded as a representative volume element (RVE), whose size must be sufficiently large to appropriately represent the microstructure, yet sufficiently small to represent a point at the macrostructure [4]. Said RVE can be regular, as the one shown in Fig. 1a, or not (Fig. 1b) – both figures present bidimensional microstructures, as cross-sections with a plane perpendicular to the fiber length.

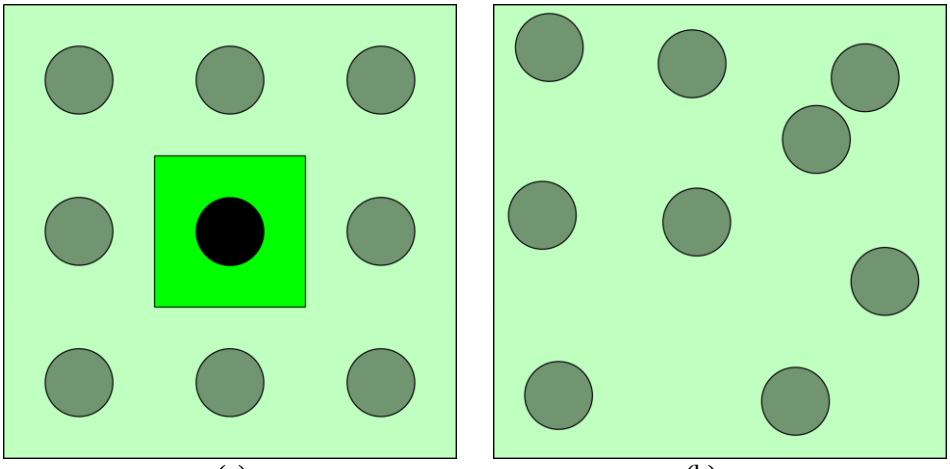

(a) (b)

Figure 1 – Composite microstructural models: (a) regular; (b) irregular.

Regular microstructures (Fig. 1a) tend to be less computationally expensive, because they can be reduced to much simpler fiber–matrix arrangements. However, real microstructures are normally irregular, being also influenced by the manufacturing process [6]. As local stress concentrations depend on the fiber arrangement [7], the necessity of analyzing irregular microstructures is clear.

Such microstructures may be interpreted as point patterns (random distributions of objects throughout specified areas called windows), which may be described through Point Process Statistics techniques, as done in [7], for example; this effectively considers the fiber centers as said randomly distributed points. These spatial distributions, although not regular, also fail to exhibit complete spatial

randomness (CSR) [8,9], in which a given point can be in any location within the window with equal probability and independently from all the other points [7]; furthermore, the simple imposition of constraints on fiber centers to ensure fiber impenetrability in random arrangements (simple hard-core model) is also unsuitable for real microstructures [10].

As CSR and simple hard-core models are ruled out as possible models for irregular microstructures, many procedures have been proposed in the literature for the generation of those fiber arrangements. Said procedures may be grouped in two broad categories: numerical generation or image processing [5]. The first category involves fully computational methods [6,10-12], whereas the second necessarily employs experimental images of the real microstructure and image processing techniques [8,9], even if the final microstructure is to be computationally generated; this is especially true if the final algorithm performs pattern reconstruction, i.e., generation of a pattern whose statistical summary characteristics are as close as possible to those of the real pattern [13].

The optimization algorithm for pattern reconstruction presented in [13] is employed here, having been implemented in R [14] with package "spatstat" [15], with adaptations for generating fiber arrangements. The following sections outline the final algorithm and preliminary verification results.

2. METHODOLOGY

2.1. Theory

Prior to presenting the employed algorithm, it is important to define the Point Process Statistics tools employed herein for pattern characterization and reconstruction; as these tools are functions, parametrized in coordinate r, they are denoted functional statistics. The ones employed in this work are defined below, according to [13], with $\mathcal{P}$ denoting probability, $\mathcal{E}$ representing an expected value, N being the number of points in a given set, μ being the point density (number of points per unit area, commonly denoted pattern intensity), and $\mathscr{b}(\boldsymbol{o}, r)$ representing a circle of radius r centered at a position of coordinates $\boldsymbol{o}$. Also, the subscript o denotes that a probability or expected value is calculated given that there is a point pattern at coordinates $\boldsymbol{o}$, whereas the symbol $\{o\}$ represents a set containing only said point.

- Spherical contact distribution function, $H(r)$: cumulative probability distribution of the minimum required radius r for a circumference centered at the origin to touch a point of the pattern, according to Eq. 1.

$$H(r) = 1 - \mathcal{P}\{N[\mathscr{b}(\boldsymbol{o}, r) = 0]\} \tag{1}$$

- Nearest neighbor distance distribution function $D(r)$: cumulative probability distribution of the distance between a typical point and its nearest neighbor, according to Eq. 2. In the case of fibers in a matrix, this distance is taken between fiber centers.

$$D(r) = \mathcal{P}_o\{N[\mathscr{b}(\boldsymbol{o}, r) \setminus \{o\}] > 0\} \tag{2}$$

- Ripley's K-function $K(r)$ and Besag's L-function, $L(r)$: the former is related to the mean number of points inside a circle of radius r centered at a typical point (which, in turn, is not counted), according to Eq. 3, whereas the latter is closely related to Ripley's K-function through Eq. 4.

$$K(r) = \frac{1}{\mu}\mathcal{E}_o\{N[\mathscr{b}(\boldsymbol{o}, r) \setminus \{o\}]\} \tag{3}$$

$$L(r) = \sqrt{\frac{K(r)}{\pi}} \tag{4}$$

- Pair correlation function $g(r)$: contains the same statistical information as Ripley's K-function and Besag's L-function, according to Eq. 5, being related to the probability of a point existing between two infinitesimally close circles of radius r centered at a typical point.

$$g(r) = \frac{1}{2\pi r}\frac{dK(r)}{dr} \tag{5}$$

Functions $H(r)$, $D(r)$, $K(r)$ and $g(r)$ are illustrated in Figures 2a through 2d below.

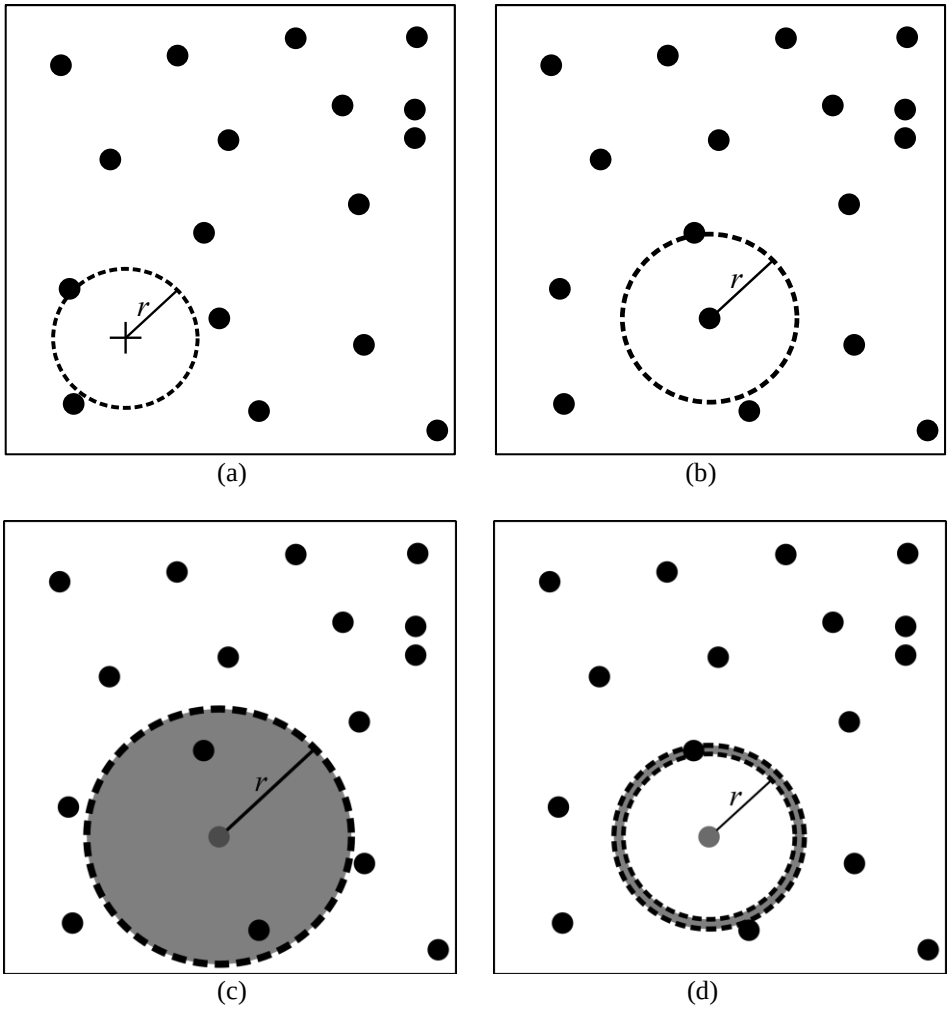

(a) (b) (c) (d)

Figure 2 – Functional statistics for pattern characterization and reconstruction: (a) $H(r)$; (b) $D(r)$; (c) $K(r)$; (d) $g(r)$

2.2. Pattern reconstruction algorithm

The algorithm presented in [13] starts from a first trial pattern having already the final number of fibers with distances between one another no greater than the minimum one measured from the reference pattern. This first trial pattern, in contrast to the final one, can be a simple hard-core one, and is, indeed, generated as such by spatstat through a simple procedure.

Afterwards, the statistics of the trial pattern are compared to those from a reference pattern, providing a value for some cost functional. Following that, the trial pattern is optimized by randomly

moving its fiber centers, in order to minimize the cost functional, i.e., to make the trial pattern statistics as close as possible to those of the reference pattern. This reference pattern is preferably obtained from experiments, but, in the verification results presented here, pattern "cells" [16], already present in spatstat, was employed.

The algorithm follows the flowchart in Fig. 3. As hypotheses, the pattern is assumed to continue far beyond the RVE while keeping its statistical characteristics; also, the arrangement is assumed statistically homogeneous (translation-invariant), isotropic (rotation-invariant, which implies a transversely isotropic composite), and periodic.

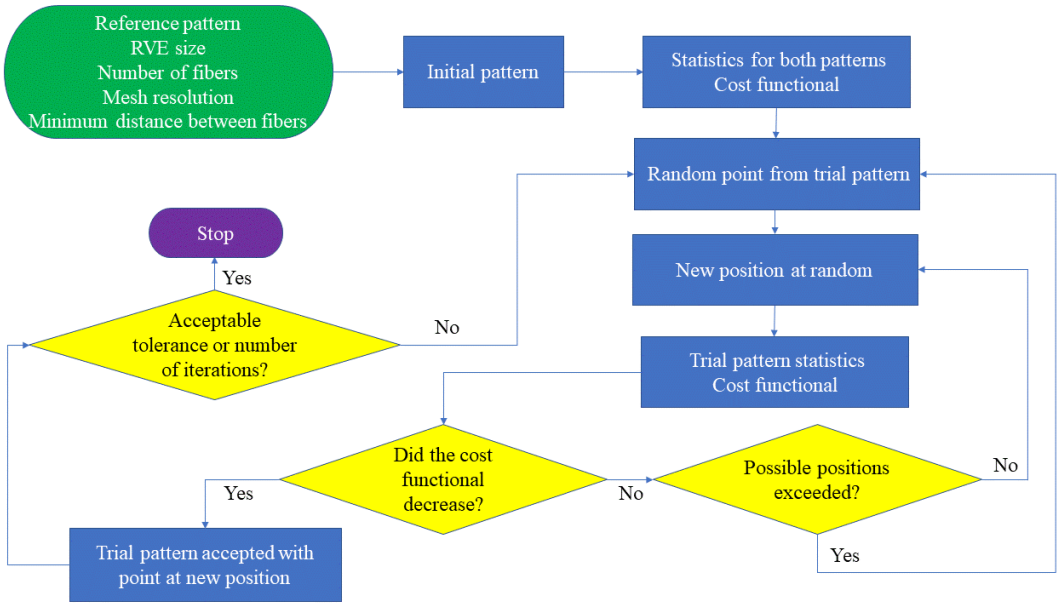

Figure 3 – Microstructure generation algorithm flowchart.

In each iteration, a random point (fiber center) is selected and moved to a random position within a mesh, whose resolution is given before the run. Moreover, uniform random noise (up to 40% of the spacing between mesh locations) is added to this trial position to prevent point superposition.

Four characteristics are employed as optimization criteria: $D(r)$ – as it affects the material stresses [7]; $L(r)$ – as it describes longer-range interactions between points and is more tractable than Ripley's K-function [13]; $H(r)$ – as it complements the information provided by the other two functions [13]; and the minimum distance between fibers (r_{min}) – penalizes patterns not respecting its admissible value, given before the run. Nevertheless, for the optimization procedure, $L(r)$ is normalized so that its maximum is 1,0, which is already true for the other two functions. The three functional statistics, collectively referred to as f_k, are calculated with appropriate edge corrections (because of the finite RVE size): $H(r)$ and $D(r)$ are calculated in reduced windows, whereas $L(r)$ takes periodicity into account. Thus, the cost functional, $\mathcal{F}$ is written Eq. 6, adapted from [13]:

$$\mathcal{F} = \sum_{k=1}^{3} \sum_{i=0}^{N_k} \left[f_k(r_{ik}) - f_k^0(r_{ik}) \right]^2 + \frac{1}{r_{min}^0} \langle r_{min} - r_{min}^0 \rangle \tag{6}$$

Above, N_k represents the number of values r_{ik} in which each f_k is calculated. Quantities calculated for the reference pattern are marked with a "0" superscript, whereas their values for the trial pattern are left with no superscript; in particular, r_{min}^0 is the minimum admissible distance between fibers, which can come from the reference pattern or be given arbitrarily. In addition, the symbol "⟨⟩"

represents adapted Macaulay brackets, shown in Eq. (7). Furthermore, to ensure periodicity (fiber impenetrability at the RVE edges), the distance r_{min} was calculated with the torus metric [13]: said metric, δ, measures the distance between two points $A = (x_1^A, x_2^A)$ and $B = (x_1^B, x_2^B)$ according to Eq. (8) [13], considering a rectangular RVE with sides of lengths l_1 and l_2.

$$\langle y \rangle = \frac{1}{2}(|y| - y) = \begin{cases} 0, & y \geq 0 \\ -y, & y < 0 \end{cases} \tag{7}$$

$$\delta = \sqrt{\left(\min\left\{\left|x_1^A - x_1^B\right|, l_1 - \left|x_1^A - x_1^B\right|\right\}\right)^2 + \left(\min\left\{\left|x_2^A - x_2^B\right|, l_2 - \left|x_2^A - x_2^B\right|\right\}\right)^2} \tag{8}$$

3. RESULTS

The algorithm was employed for reconstruction of the pattern cells [16], having 42 points (considered as fiber centers), with a clear minimum distance between them, in a unit rectangle window. Here, the minimum admissible distance between fibers, r_{min}^0, was set to be 0.06 for convenience, which is smaller than the minimum distance between points in the reference pattern, whether measured through the Euclidean metric (0.084) or the torus metric (0.063). In other words, this means that the fibers represented by the pattern could have a diameter (when supposed uniform) of up to r_{min}^0, in which case they would be allowed to at most contact one another through a single point.

The final pattern and the reference one are presented in Fig. 4.

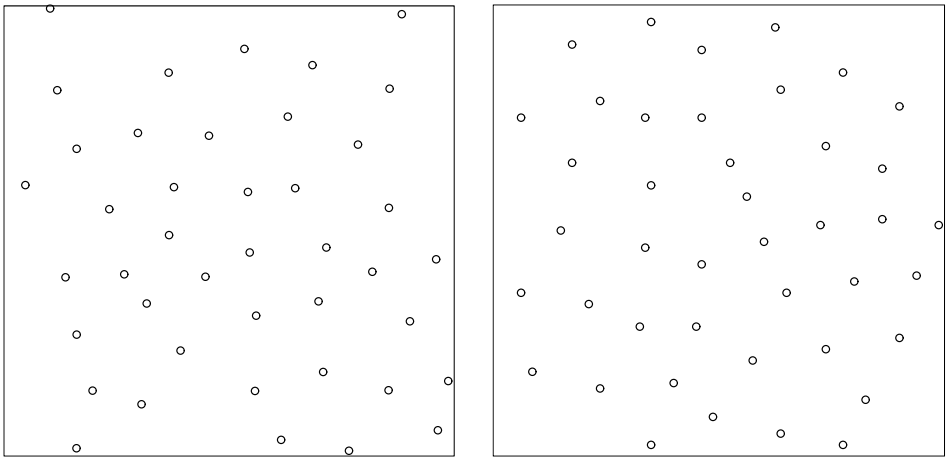

(a) (b)

Figure 4 – Point patterns for algorithm verification: (a) reconstructed; (b) reference.

The total runtime was 1.12 hours, and the final cost functional was 0.204; the respective cost contributions are given in Tab. 1: as it can be seen from said table, r_{min} had no contribution to the final cost, meaning that the minimum distance between fibers in the final pattern was satisfactory, considering the chosen value for r_{min}^0.

Table 1 – Optimization cost contributions

Cost contribution	$\boldsymbol{H(r)}$	$\boldsymbol{D(r)}$	$\boldsymbol{L(r)}$	$\boldsymbol{r_{min}}$
Absolute	0.007	0.123	0.074	0.0
Relative (%)	3.43	60.29	36.27	0.0

Figures 5 through 8, produced in R [14], compare $H(r)$, $D(r)$, $L(r)$ and $g(r)$ for the reference and the reconstructed patterns; in the former three figures, the cost contributions presented in Tab. 1 can be seen graphically.

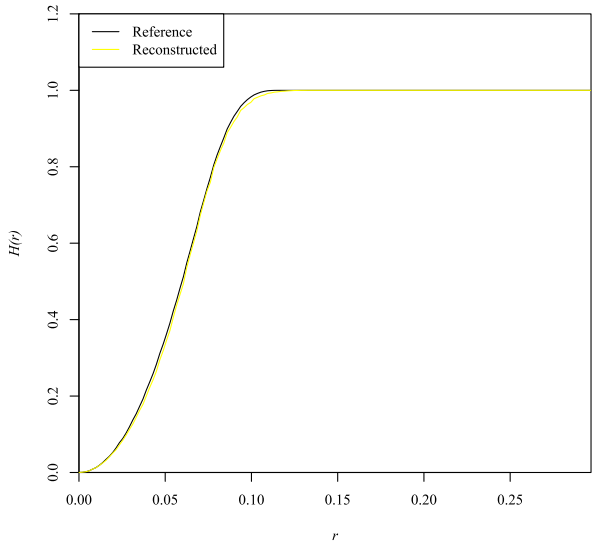

Figure 5 – $H(r)$ for the reference and reconstructed patterns.

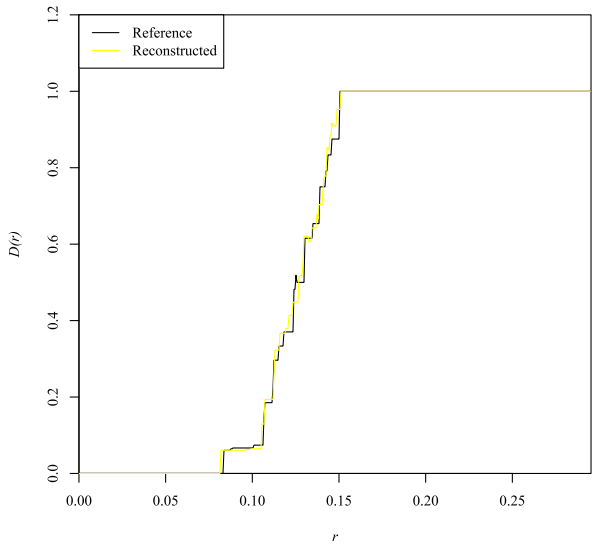

Figure 6 – $D(r)$ for the reference and reconstructed patterns.

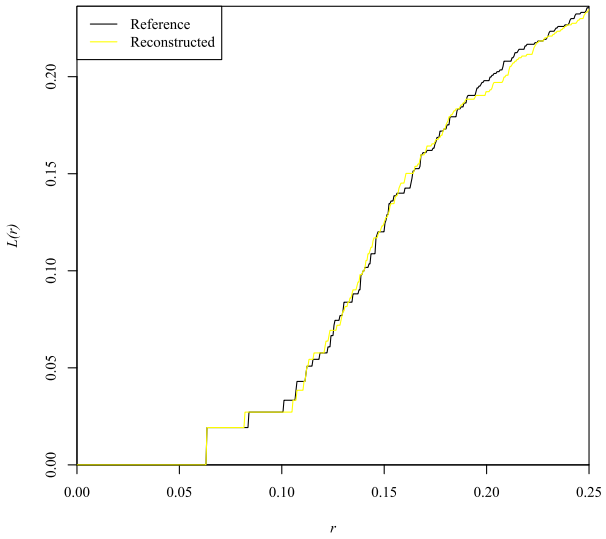

Figure 7 – $L(r)$ for the reference and reconstructed patterns.

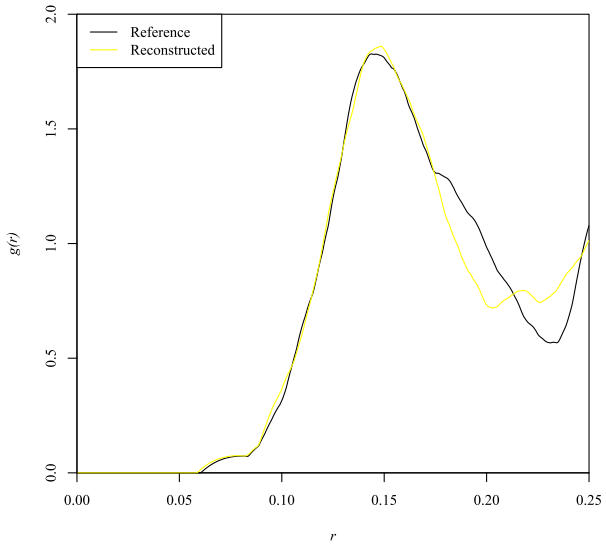

Figure 8 – $g(r)$ for the reference and reconstructed patterns.

From the figures, the final produced pattern presented functional characteristics arguably close to those of the reference point pattern.

4. CONCLUSION

The proposed algorithm has been capable of satisfactorily reconstructing a given point pattern, although further tests are necessary to verify its performance when applied to fiber distributions with greater fiber volumetric fractions. In addition, the isotropy hypothesis is currently being studied, to verify more rigorously if it holds for both the reference and the reconstructed patters.

Future works include extending the procedure to the generation of microstructures with voids, effectively reconstructing patterns with more features.

ACKNOWLEDGEMENTS

Volnei Tita would like to thank the National Council for Scientific and Technological Development (CNPq process number: 310159/2022-9).

REFERENCES

[1] W. Tan, B.G. Falzon, L.N.S. Chiu et al. Predicting low-velocity impact damage and compression after impact (CAI) behaviour of composite laminates. *Composites Part A: Applied Science and Manufacturing*, v. 71, p. 212–226. (2015).
[2] R. Talreja. Assessment of the fundamentals of failure theories for composite materials. *Composites Science and Technology*, v. 105, p. 190-201. (2014).
[3] M.J. Bogdanor, C. Oskay, S.B. Clay. Multiscale modeling of failure in composites under model parameter uncertainty. *Computational Mechanics*, v. 56, p. 389-404. (2015).
[4] G. Chatzigeorgiou, F. Meraghni, N. Charalambakis. *Multiscale modeling approaches for composites*. Elsevier Inc. Amsterdam; Oxford; Cambridge, Massachusetts. (2022).
[5] H. Ghayoor, S.V. Hoa, C.C. Marsden. A micromechanical study of stress concentrations in composites. *Composites Part B: Engineering*, v. 132, p. 115-124. (2018).
[6] A.R Melro, P.P. Camanho, S.T. Pinho. Generation of random distribution of fibres in long-fibre reinforced composites. *Composites Science and Technology*, v. 68, p. 2092-2102. (2008).
[7] R. Pyrz. Correlation of microstructure variability and local stress field in two-phase materials. *Materials Science and Engineering: A*, v. 177, p. 253-259. (1994).
[8] V.N. Bulsara, R. Talreja, J. Qu. Damage initiation under transverse loading of unidirectional composites with arbitrarily distributed fibers. *Composites Science and Technology*, v. 59, p. 673-682. (1999).
[9] T.J. Vaughan, C.T. McCarthy. A combined experimental-numerical approach for generating statistically equivalent fibre distributions for high strength laminated composite materials. *Composites Science and Technology*, v. 70, p. 291-297. (2010).
[10] A. Sudhir, R. Talreja. Simulation of manufacturing induced fiber clustering and matrix voids and their effect on transverse crack formation in unidirectional composites. *Composites Part A: Applied Science and Manufacturing*, v. 127, p. 105620. (2017).
[11] S.A. Elnekhaily, R. Talreja. Damage initiation in unidirectional fiber composites with different degrees of nonuniform fiber distribution. *Composites Science and Technology*, v. 155, p. 22-32. (2018).
[12] G. Li, F. Sharifpour, A. Bahmani et al. A new approach to rapidly generate random periodic representative volume elements for microstructural assessment of high volume fraction composites. *Materials and Design*, v. 150, p. 124-138. (2018).
[13] J. Illian, A. Penttinen, H. Stoyan et al. *Statistical analysis and modelling of spatial point patterns*. John Wiley & Sons, Ltd. Chichester, UK. (2008).
[14] R Core Team. *R: a language and environment for statistical computing*. Vienna, Austria. (2008).
[15] A. Baddeley, E. Rubak, R. Turner. *Spatial point patterns: Methodology and applications with R*. Chapman and Hall/CRC Press. London, UK. (2015).
[16] B. D. Ripley. Modelling spatial patterns. *Journal of the Royal Statistical Society: Series B (Methodological)*, v. 39, n. 2, p. 172-192. (1977).

RESPONSIBILITY NOTICE

The author(s) is (are) the only responsible for the printed material included in this manuscript.